Epitaxial Fe-Ge thin films on Ge(111): Morphology, structure, and magnetic properties versus stoichiometry

R. Jaafar,[1] D. Berling,[1] D. Sébilleau,[2] and G. Garreau[1,*]

[1]*Institut de Science des Matériaux de Mulhouse, CNRS-LRC 7228, Université de Haute-Alsace, Mulhouse, France*

[2]*Equipe de Physique des Surfaces et Interfaces, Institut de Physique de Rennes, UMR CNRS-UR1 6251, Université de Rennes-1, 35042 Rennes Cedex, France*

(Received 15 December 2009; revised manuscript received 25 February 2010; published 12 April 2010)

We have studied the growth and magnetic properties of thin Fe-Ge films synthesized (codeposited at room temperature and postannealed at 250 °C) on Ge(111) wafers versus stoichiometry. Morphology and crystal structure have been investigated *in situ* by means of scanning tunneling microscopy, low-energy electron diffraction, and x-ray photoelectron diffraction and *ex situ* with x-ray diffraction. The magnetic properties were characterized *ex situ* by conventional polar and longitudinal magneto-optical Kerr effect and transverse biased initial inverse susceptibility and torque measurements. It is found that the growth is epitaxial for Ge content up to ~48 at. % (~$Fe_{1.1}Ge$ composition). In particular, the film is homogeneous and flat and adopts a crystalline structure of hexagonal symmetry derived from the $B8_2$ (Ni_2In) structure over a wide stoichiometry range extending from Fe_2Ge to $Fe_{1.1}Ge$. The epitaxial orientation between the Ge substrate and the germanide layer is (0001)Fe-Ge∥(111)Ge with $[11\bar{2}0]$Fe-Ge∥$[\bar{1}10]$Ge. We found however that the surface periodicity and the out-of-plane lattice parameter c evolve within this stoichiometry range and two distinct stoichiometry regimes appear on both sides of a critical stoichiometry (~$Fe_{1.5}Ge$). Indeed, from Fe_2Ge to $Fe_{1.5}Ge$ the surface periodicity is $p(2\times2)$ and c continuously decreases with Fe content, whereas from $Fe_{1.5}Ge$ to $Fe_{1.1}Ge$ the surface periodicity is $(\sqrt{3}\times\sqrt{3})R30°$ and c remains constant. These features have been interpreted as a clear fingerprint of a minor transformation of the crystalline structure but without any change in symmetry. This structural order transformation is discussed in relation to previous results reported in the case of *macroscopic* single-crystal Fe-Ge ingots. On both sides of the wide [Fe_2Ge, $Fe_{1.1}Ge$] composition range the layer is no more homogeneous. More precisely, for higher Fe content the film contains both the above mentioned Ni_2In-derived phase and a Fe-richer phase (probably bcc Fe) whereas for higher Ge content the layer is amorphous. Magnetic characterization showed in particular that the homogeneous Ni_2In-derived epilayers are ferromagnetic with a Curie temperature that varies drastically with the stoichiometry, rising up to a high T_C value of ~450 K for the Fe-rich $Fe_{1.9}Ge$ composition. Finally, whatever the stoichiometry, the magnetic easy axis of the homogeneous phase lies in the film plane and a small uniaxial anisotropy is superimposed on a sixfold order one that results from the hexagonal symmetry of the crystallographic structure.

DOI: 10.1103/PhysRevB.81.155423 PACS number(s): 68.55.−a, 68.37.Ef, 61.05.js, 81.05.Bx

I. INTRODUCTION

Ferromagnetic/semiconductor (FM/SC) hybrid structures are interesting candidate for the realization of spintronic devices. These potentialities led in the past two decades to an impressive number of studies concerning the growth and the magnetic properties of epitaxial thin films of 3*d* transition metals on semiconductor single crystal. Most of them focused on Fe epilayers grown on GaAs (Ref. 1) and ZnSe (Ref. 2) substrates. On the other hand, since 2000 very few papers deal with the growth of 3*d* ferromagnet directly on Si or Ge despite the fact that Si is overwhelming in the semiconductor technology and Ge is compatible in the integration of Si based electronic. The major reason of this is that the growth of elemental FM (Co, Fe, etc.) directly on Si (Ge) leads to the formation of silicide (germanide) compounds at the FM/SC interface. These (uncontrolled) interfacial layers are nonmagnetic even at low temperature (the so-called magnetically dead layers) and therefore detrimental to the electron spin injection from the FM to the SC. To reduce this intermixing the insertion of a thin insulating tunnel barrier has been proposed in the case of Fe deposited on Si.[3] Another possible way to prevent these nonmagnetic alloys could be the growth of ferromagnetic intermetallic FM-SC alloys directly on the semiconductor SC. Indeed, we may expect that these intermetallic compounds that are usually synthesized in stable bulk phases at high temperature are much less reactive with the semiconductor than pure elemental FM. However, the crystalline intermetallic compounds that show ferromagnetic order above room temperature (RT) are scarce. Up to now, Fe_3Si,[4] $Fe_{3-x}Mn_xSi$,[5] and Mn_5Ge_3 (Ref. 6) thin ferromagnetic intermetallic films have been successfully *epitaxially* grown on Ge(111). Nevertheless no data on the magnetism and the reactivity at the interface (or in the ultrathin thickness regime) have been reported so far for these systems. Very recently we have shown that room-temperature ferromagnetic $Fe_{1.7}Ge$ thin epilayers of high quality can be synthesized on Ge(111) with no magnetically dead layers at the interface up to at least 300 °C.[7]

Let us now consider the equilibrium phase diagram of the binary Fe-Ge alloy as reported in Fig. 1(a). In fact, the Fe-Ge system is of particular interest because of the formation of different magnetically ordered phases in the wide range of compositions. Besides the ferromagnetic Fe_3Ge phase that adopts either a hexagonal (the high temperature ε phase) or a face-centered-cubic (the low temperature ε′ *phase*) crystal

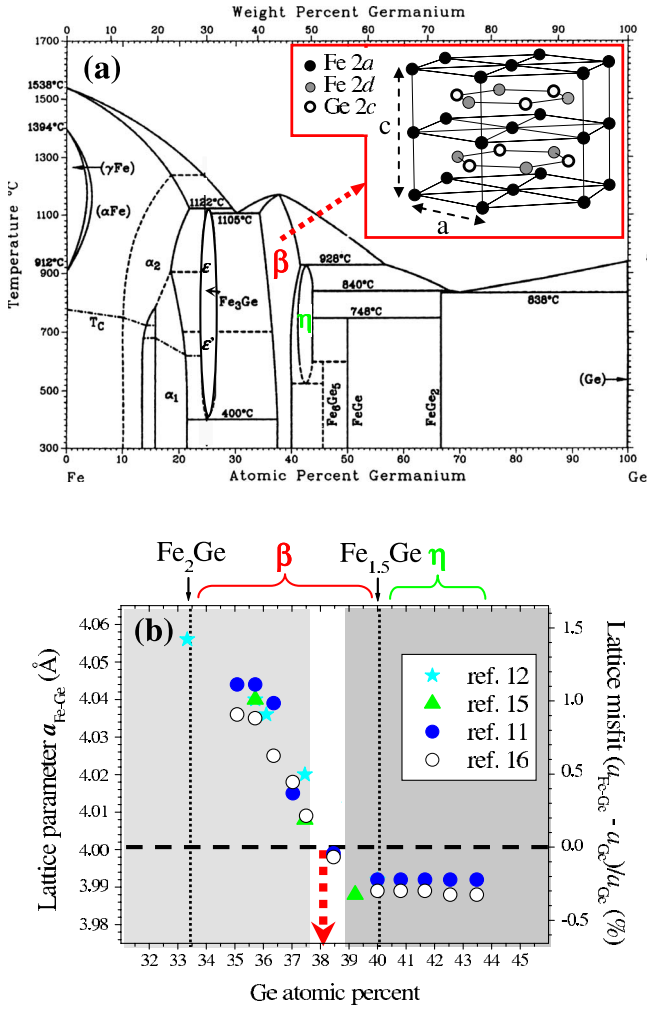

FIG. 1. (Color online) (a) The equilibrium Fe-Ge phase diagram and (inset) the hexagonal $B8_2$-β phase for the stoichiometry Fe_2Ge (without vacancy). One Fe atom (Fe 2*a*) is located in the Wyckoff position 2*a* (0, 0, 0), one Fe atom (Fe 2*d*) occupies the position 2*d* (1/3, 2/3, 3/4), and the Ge atom (Ge 2*c*) is found in the 2*c* (1/3, 2/3, 1/4) position. (b) In-plane lattice parameter *a* of the hexagonal $B8_2$-derived phases (i.e., β and η phases) versus Ge atomic percent in the case of macroscopic Fe-Ge ingots. The horizontal dashed line corresponds to the lattice parameter a=4.001 Å of the (111) germanium plane. The dotted arrow indicates the Fe-Ge composition for which perfect lattice matching is expected between β-Fe-Ge(0001) layers and Ge(111) substrate.

structure, most of the papers reported in the literature focused on the antiferromagnetic FeGe and $FeGe_2$ phases. For the narrow stoichiometry range extending from about Fe_2Ge to $Fe_{1.5}Ge$ the stable bulk phase adopts the hexagonal β phase derived from the $B8_2$-Ni_2In structure [inset of Fig. 1(a)]. This phase has been investigated by different groups in the past and has led to a wide spread of conflicting results.[8–18] It was synthesized as macroscopic single-crystal ingots after several days or weeks of heat treatment. It consists of alternate planes of Fe (Fe 2*a*) atoms and mixed Fe (Fe 2*d*) plus Ge (Ge 2*c*) atoms along the *c* direction. This phase is stabilized by the formation of vacancies (mainly) on the Fe 2*d* sites when the composition evolves from Fe_2Ge to $Fe_{1.5}Ge$. Indeed, the progressive formation of the vacancies leads to a continuous increase of the Fe-Ge distance in the mixed Fe 2*d* plus Ge 2*c* atom planes, this distance being too short (~2.30 Å) in the ideal (without vacancy) $B8_2$ structure with respect to the shortest Fe-Ge distances (between ~2.37 Å for the η phase and 2.58 Å for the ε phase) of the other bulk stable Fe-Ge phases. Malaman *et al.*[16] showed that the β-phase space group symmetry is not $P6_3/mmc$ as proposed in Refs. 8 and 10–12 but close to $P\bar{3}m1$ as suggested by Forsyth and Brown.[9] It has been found that the Curie temperature of this β phase varies significantly versus stoichiometry from ~520 K for $Fe_{1.85}Ge$ to 430 K for $Fe_{1.5}Ge$. As depicted in Fig. 1(b) the lattice parameter a_β decreases from ~4.04 Å for $Fe_{1.85}Ge$ to ~3.99 Å for $Fe_{1.5}Ge$. It suggests clearly that Ge(111) could be an ideal substrate for the growth of this hexagonal Fe-Ge phase since the lattice parameter of Ge in the hexagonal (111) plane is ~4.001 Å. A perfect lattice matching is indeed expected for a composition with about 38% Ge atomic concentration as marked by the dotted arrow in Fig. 1(b). Thus, the relatively high Curie temperature, the high magnetic Fe moments [$\sim 2.1\mu_B$ for Fe 2*a* and $\sim 1.4\mu_B$ for Fe 2*d* (Ref. 15)], and the tiny lattice mismatch (between −0.3% and +1.2% according to the Ge content) with the Ge substrate as well are appealing facts that make the growth of single-crystal β layers on Ge an attractive challenge. In addition, we think that this bulk β phase has to be reinvestigated because of the wide spread of controversial results concerning the atom or vacancy site distribution, the magnetic moment amplitude on the two distinct Fe atomic sites, and the magnetic order as well, which can be found in the literature.

Upon increasing the Ge content (between $Fe_{1.5}Ge$ and FeGe) the germanide compound crystallizes in two phases, called η (for composition between $Fe_{1.4}Ge$ and $Fe_{1.3}Ge$) and Fe_6Ge_5 (for composition around $Fe_{1.1}Ge$), which have a close structural relation to the β phase. Indeed the η phase has also a hexagonal structure but with lattice parameters $a_\eta = 2a_\beta$ ~8.0 Å and $c = 2c_\beta \sim 5.0$ Å. This structure is not merely a superstructure related to the β phase by an order-disorder transformation but is a distinct ordered phase.[11] On the other hand the crystal structure of Fe_6Ge_5 corresponds to a relatively strongly distorted $B8_2$-type subcell (monoclinic $C2/m$ space group symmetry) with c_η=4.983 Å, b_η=3.913 Å, and a_η=4.162 Å.[16,19]

In this paper, we report on a detailed study of the growth, the structure, and the magnetic properties of thin (thickness below 40 nm) Fe-Ge layers synthesized by molecular-beam epitaxy (MBE) on Ge(111) wafers versus stoichiometry. The Fe-Ge layers were codeposited onto the Ge substrate held at RT and postannealed at ~230 °C. The structural investigation of these germanide layers has been carried out by means of scanning tunneling microscopy (STM), low-energy electron diffraction (LEED), x-ray photoelectron diffraction (XPD), and x-ray diffraction (XRD) in the θ-2θ configuration. The major result is that the germanide layer crystallizes in a hexagonal phase derived from the β phase over a wide composition range extending from ~Fe_2Ge to ~$Fe_{1.1}Ge$. Tiny changes of the atomic local order inside the layer occur within this stoichiometry range leading in particular to a sudden $p(2\times2) \rightarrow (\sqrt{3}\times\sqrt{3})R30°$ surface periodicity change at

a critical stoichiometry ($\sim Fe_{1.5}Ge$). On both sides from the [Fe_2Ge, $Fe_{1.1}Ge$] stoichiometry window the layer is no more homogeneous; i.e., it contains several phases. Magnetic measurements performed mainly with magneto-optical Kerr effect (MOKE)-based setup show that the Curie temperature of the homogeneous hexagonal phase strongly depends on the stoichiometry and rises up to 450 K for composition close to Fe_2Ge. Finally the structural and magnetic properties of our epilayers will be discussed in the light of the aforementioned studies performed in the past on *macroscopic* single-crystal Fe-Ge ingots.

II. EXPERIMENT

Sample preparation, as well as LEED, STM, and XPD measurements, was carried out in three interconnected ultrahigh vacuum (UHV) chambers with pressure below 1×10^{-10} mbar. The Fe-Ge thin films were grown on Ge(111) using homemade Fe and Ge thermal evaporators. Ge(111) substrates were first cut from nominally flat single side polished (p doped $\rho \sim 0.2\ \Omega$ cm) wafers. After a short rinse in acetone, ethanol, and hydrogen peroxide, the substrate was inserted into the UHV chamber and degassed by direct heating up to 800 K for 10 h. After repeated flashes at 1000 K for increasing durations (up to 1 min), the substrate was cooled rapidly to 900 K and then slowly (at a rate of 1 K/s) down to RT. A sharp $c(2\times 8)$ pattern was observed by LEED and STM images indicate that the surface consists of irregular monoatomic step terraces of several tens of nanometer width. Fe and Ge were first codeposited onto Ge(111) substrate held at RT. Then, the sample was annealed 12 h around 230 °C. The thickness of the germanide layer will be given in nominal Fe coverage [$0 < t_{Fe} < 200$ monolayers (MLs), 1 ML corresponding to the atomic density of a Ge(111) plane, i.e., $\sim 7.2 \times 10^{14}$ atoms/cm^2]. Fe and Ge deposition rates were determined by water-cooled quartz crystal microbalances and were adjusted to a few tenths of ML/min at the desired stoichiometric ratio. From the calibrated microbalances, both the y parameter of the nominal Fe_yGe stoichiometry and the film thickness are given with a precision better than 10%. As the stoichiometry is a *crucial* parameter in this study we controlled it more precisely, before and after the annealing treatment, through the measurement of the ratio between the Fe $2p$ and Ge $3d$ photoelectron line intensities. From this we estimate that the *relative* stoichiometry (i.e., from one sample to the other) is given with an uncertainty below 5%. The film composition will be expressed both as Fe_yGe (for clarity) and as $Fe_{100-x}Ge_x$ (x=Ge atomic percent)[20] in order to facilitate the comparison between our results and part of the "old" literature. XPD measurements were carried out using a 125 mm radius hemispherical analyzer operating at an angular resolution of about 2°. XPD scans were obtained by measuring the intensity of the Fe $3p$ and Ge $3d$ core levels excited with an unmonochromatized Al $K\alpha$ x-ray source ($h\nu = 1486.6$ eV). Polar angular scans were recorded along azimuths of high symmetry. The polar angle θ is referred to the surface normal of the sample. XPD calculations were computed using the MSSPEC package.[21] This package allows us to model several spectroscopies where the electron is the probe using different algorithms. STM measurements were performed with a commercial RT-operating microscope (STM atomic force microscopy Omicron). The STM tungsten tips were electrochemically etched and cleaned *in situ* by e-beam heating. The STM images were collected in the constant-current mode. After completion of the *in situ* LEED, STM, and XPD analyses, the sample was covered at RT by a protective 30-Å-thick Ge layer for the magnetic characterization and the XRD experiments. XRD measurements were performed in the θ-2θ configuration with either a monochromatized Cu $K\alpha$ source ($\lambda = 1.541$ Å) or a unmonochromatized Cu radiation. The magnetic properties were investigated *ex situ* by means of two distinct MOKE polarimeters. With the first MOKE magnetometer, magnetization loops were collected from 20 to 500 K in longitudinal geometry, i.e., with the external magnetic field applied in the film plane and in the incidence plane at the same time. In order to determine accurately the different tiny contributions of the magnetic in-plane anisotropy, we have performed transverse biased initial inverse susceptibility and torque (TBIIST) measurements with a RT-operating MOKE setup. This TBIIST method is described in detail in Ref. 22. For both MOKE magnetometers, the incidence angle of the laser beam ($\lambda = 633$ nm) is about 45° with respect to the sample normal.

III. RESULTS AND DISCUSSION

A. Growth and structure

1. Layer morphology

We have first performed a detailed STM analysis of the film morphology versus film thickness and stoichiometry. Since the evolution of the film morphology as a function of thickness is very similar within the stoichiometry range [Fe_2Ge, $Fe_{1.1}Ge$] investigated here, we will focus only on a fixed composition, namely, $Fe_{1.2}Ge$ ($\approx Fe_{55}Ge_{45}$). The modification of the surface morphology versus nominal Fe thickness is depicted in Fig. 2. After deposition of 0.3 ML [Fig. 2(a)] less than 10% of the surface is covered by small disconnected Fe-Ge islands (bright area) surrounded by the pristine Ge substrate (dark areas) that presents small randomly distributed domains of $p(2\times 2)$ or $c(2\times 8)$ periodicity. We clearly observe that the Fe-Ge clusters have a height distribution that is roughly bimodal. Indeed one half of the islands (the smaller ones) are nearly triangular with an apparent height between 2 and 3 Å, whereas the other half consists of (5–6)-Å-thick clusters. Inside the Ge substrate area small domains [marked by the circle in the inset of Fig. 2(a)] are also visible. These domains have a typical loop shape that results likely from the presence of a Fe atom located below and at the center of six Ge adatoms as observed previously in the case of small Co deposit on Si(111).[23] We found that the mean lateral extension of the Fe-Ge islands increases continuously with the coverage and, after 1 ML coverage [Fig. 2(b)], only the (5–6)-Å-thick islands are present. These flat and disconnected clusters cover about 50% of the sample surface. Above 1 ML, the island thickness increases with coverage and the island coalescence occurs around 3 ML. Above 5 ML coverage, most of the sample surface is covered

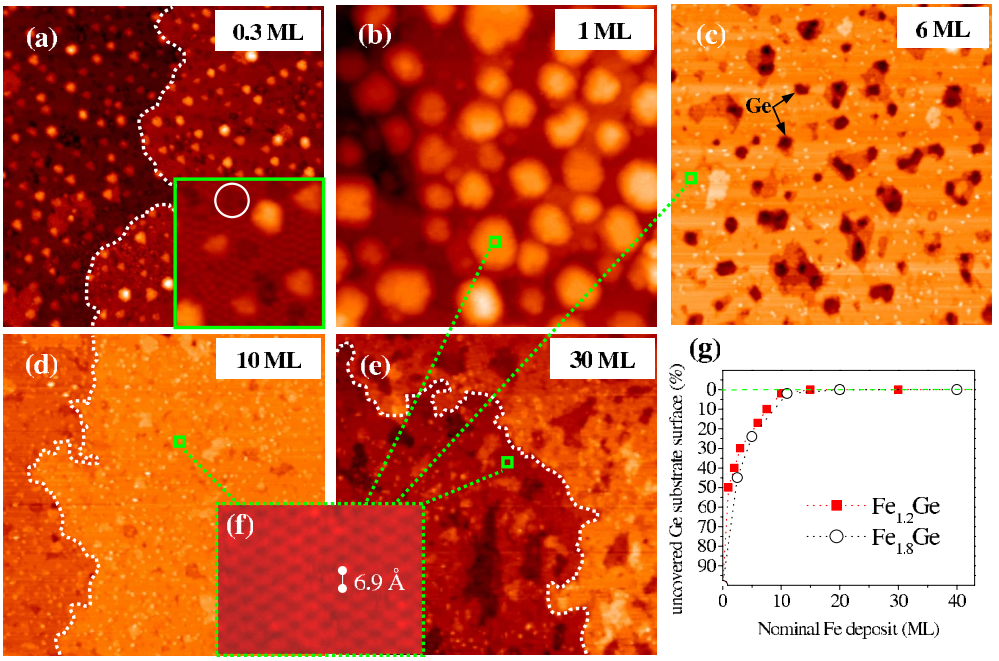

FIG. 2. (Color online) A series of STM images showing the evolution of the surface morphology of 230 °C annealed $Fe_{1.2}Ge$ films as a function of nominal Fe deposit (0–30 ML). All the images are taken at a positive sample bias of 2 V and a tunneling current of 0.1 nA. The surface area is 150×150 nm^2 for (a)–(e) and the atomically resolved zoom [inset (f)] reflects a $(\sqrt{3}\times\sqrt{3})R30°$ periodicity. The white dotted line in (a), (d), and (e) delimits two consecutive Ge(111) substrate terraces separated by a step height of ~3.3 Å. The curves in (g) indicate the uncovered Ge substrate surface area versus nominal Fe deposit for two distinct compositions, $Fe_{1.8}Ge$ and $Fe_{1.2}Ge$.

by the Fe-Ge layer. This is illustrated in Fig. 2(c) collected after 6 ML deposit. The Fe-Ge layer represents about 80% of the surface. The darkest areas that are located ~1.5 nm below the top iron germanide surface correspond to the pristine Ge substrate. These uncovered Ge substrate areas decrease with further deposition and no pinholes are visible for coverage higher than about 15 ML [Fig. 2(g)]. Let us focus now on the Fe-Ge layer surface. As clearly visible on images (b)–(f) of Fig. 2, the germanide layer is atomically flat whatever the coverage. Indeed only three height levels are present for a given pristine Ge substrate terrace [delimited by a white dotted line in Figs. 2(d) and 2(e)] and the roughness (rms) is typically below 2–3 Å (for 50×50 nm^2 area). In fact, most of the germanide surface is on the same height level and only some small areas are either 2.5 Å above or 2.5 Å below this reference level. It indicates that two consecutive germanide terraces are separated by about 2.5 Å along the surface normal. It is relevant for the following to note that all the above mentioned results concerning the thickness dependence of the surface morphology have been obtained for any composition between Fe_2Ge and $Fe_{1.1}Ge$.

2. Surface periodicity

The surface periodicity versus film thickness and stoichiometry has been investigated with STM and LEED. All the results are summarized in Fig. 3. Unlike the morphology we found first that the germanide surface periodicity depends on the composition within the stoichiometry range [$Fe_{1.1}Ge$, Fe_2Ge]. Indeed for composition between ~$Fe_{1.1}Ge$ and ~$Fe_{1.5}Ge$ (region labeled III in Fig. 3) both LEED patterns and atomically resolved STM images [Fig. 2(f)] reflect a $(\sqrt{3}\times\sqrt{3})R30°$ periodicity. The periodicity turns into $p(2\times2)$ for composition between $Fe_{1.5}Ge$ and Fe_2Ge (region II). It is worth noting that the periodicity change does not affect the honeycomb structure revealed by atomically resolved

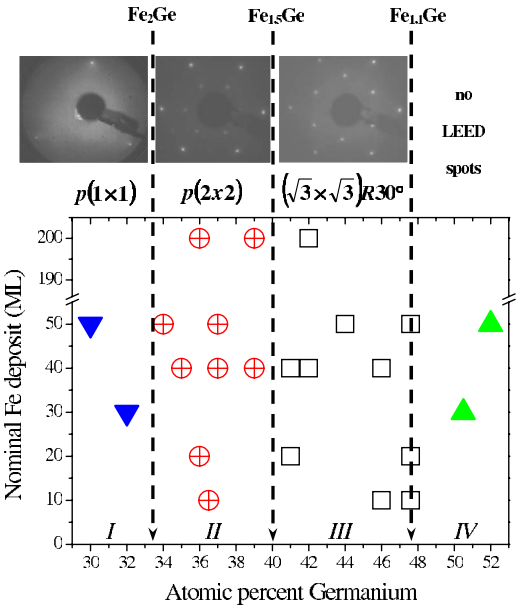

FIG. 3. (Color online) Evolution of the surface periodicity as a function of stoichiometry and thickness. The three LEED patterns have been measured with 57 eV electron energy. The vertical dashed arrows delimit four regions labeled I–IV of distinct surface periodicity: $p(1\times1)$ for I, $p(2\times2)$ for II, $(\sqrt{3}\times\sqrt{3})R30°$ for III, and no periodicity for IV.

STM images. Indeed both the enlarged images of Figs. 1(e) and 2 from Ref. 7 exhibit a hexagonal network but with a distinct lateral spacing d—~0.7 nm for $(\sqrt{3}\times\sqrt{3})R30°$ against ~0.8 nm for $p(2\times2)$—between two consecutive bright (or depressed) "spots." Figure 3 also shows that for a fixed composition the periodicity remains unchanged whatever the thickness of the continuous germanide layer. We have also recorded the LEED intensity spectra—the so-called $I(V)$ of first-order integer spots—(10), (11), (01), and $(\bar{1}0)$—as a function of electron energy (in the 30–300 eV range) for samples with either $(\sqrt{3}\times\sqrt{3})R30°$ or $p(2\times2)$ periodicity. We observed that for each periodicity the four $I(V)$ curves (not shown here) are nearly identical. It clearly shows that the symmetry of the surface layer is hexagonal for the wide $[Fe_2Ge, Fe_{1.1}Ge]$ stoichiometry range.

On the other hand it is no more the case on both sides of this range. Indeed for composition richer in Fe than Fe_2Ge (region I) the germanide layer is still crystallized since the LEED pattern reflects a $p(1\times1)$ periodicity. However the (left) LEED pattern in Fig. 3 clearly exhibits a threefold symmetry and the background intensity is significantly enhanced with respect to one of the two other periodicities. For samples with Ge content higher than the composition $Fe_{1.1}Ge$ (region IV) no LEED diffraction spot could be observed which suggests that the layer is amorphous or of poor crystallinity.

From the above described STM and LEED observations, it is reasonable to speculate that, over the wide $[Fe_2Ge, Fe_{1.1}Ge]$ stoichiometry range, the homogeneous germanide layer could adopt a crystallographic structure close to the hexagonal β phase mentioned earlier, with the [0001] direction along the surface normal. Indeed the observed 2.5 Å spacing between the germanide terraces is exactly half the lattice constant c along [0001], and the honeycomb network with its hexagonal symmetry is not unexpected for a lamellar structure like the β phase.[24] In fact, we have shown previously using high-resolution transmission electron microscopy (HRTEM) that the diffraction patterns are actually consistent with the hexagonal β phase structure for *the* composition $Fe_{1.7}Ge$ of $p(2\times2)$ periodicity.[7] We have also collected HRTEM images and diffraction patterns both in cross section and in plane view geometries for a sample with the $Fe_{1.2}Ge$ composition [of $(\sqrt{3}\times\sqrt{3})R30°$ periodicity]. The diffraction patterns suggest that the layer phase is also close to the β phase for this stoichiometry. Unfortunately, since (i) the 200 kV acceleration voltage of our microscope was too weak with respect to the high density of the Fe-Ge germanide layer and (ii) part of the intense Ge substrate spot positions coincide with the weak germanide spots on the diffraction patterns, we were not able to detect the tiny, if any, structural differences between samples with distinct periodicity. Thus, there is no interest to show this HRTEM analysis here.

Although our LEED (sixfold order symmetry), STM (step height), and TEM data as well collected for any stoichiometry between Fe_2Ge and $Fe_{1.1}Ge$ are fully compatible with the β structure, the sudden surface periodicity change around the composition $Fe_{1.5}Ge$ suggests however that a structural change occurs on both sides of this critical stoichiometry

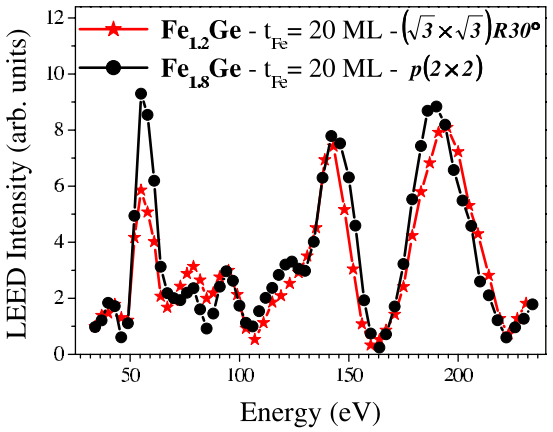

FIG. 4. (Color online) *I-V* LEED intensity curves for two compositions with distinct surface periodicity: (stars) $Fe_{1.2}Ge$ (t_{Fe}=20 ML) of $(\sqrt{3}\times\sqrt{3})R30°$ symmetry and (circles) $Fe_{1.8}Ge$ (t_{Fe}=20 ML) of $p(2\times2)$ symmetry. The intensity has been averaged over the four equivalent—(10), (11), (01), and $(\bar{1}0)$—first-order integer spots of the LEED pattern.

but without any symmetry change. We have performed LEED-$I(V)$ measurements in order to collect additional structural data. Figure 4 displays LEED-$I(V)$ spectra of the first-order integer spots[25] recorded for two distinct samples with either $p(2\times2)$ or $(\sqrt{3}\times\sqrt{3})R30°$ periodicity. It appears immediately that the intensity modulations are very similar to each other. In particular the different intensity minima (corresponding to destructive interferences) are located at the same energy for the two distinct periodicities. Thus, these $I(V)$ spectra clearly indicate that, at the depth probed by LEED, the crystal structures are very close although the samples exhibit clearly distinct LEED patterns. In addition, as the intensity minima are close to zero we may assume that the film contains only one homogeneous single-crystal phase, in agreement with the above STM analysis. An additional result may be drawn from the LEED data. The fact that the first-order integer spots $I(V)$ are nearly identical for the two distinct periodicities shows that this surface periodicity is not linked to a drastic modification of the atomic arrangement in the outermost atomic layers. Indeed, such a rearrangement in the top atomic layers should lead to a modification of the diffraction conditions. It has been observed, for instance, by Starke *et al.*[26] in the case of thin cubic CsCl $FeSi_2$ films: upon annealing above 400 °C the initially RT (1×1)-$FeSi_2$ phase transforms into a (2×2)-$FeSi_2$ phase as a result of the (2×2) Si atom network segregation on top of the $FeSi_2$ film. This (2×2) superstructure led to drastic modifications of the integer order spot $I(V)$ curves between (1×1)-$FeSi_2$ and (2×2)-$FeSi_2$, although the "buried" layer keeps both the same CsCl structure and the same stoichiometry. Thus, the clear surface periodicity change detected by STM and LEED around $Fe_{1.5}Ge$ composition corresponds very likely to a transition between two phases that have very similar crystallographic structure. As this critical stoichiometry is the same as the one for which macroscopic Fe-Ge ingot phase changes from β to η (that have closely related crystallographic structures), it is tempting to propose that the same structural change occurs in the case of our thin germanide layers. This will be discussed later.

Lastly, it is amazing at first glance that the LEED-$I(V)$ spectrum remains nearly unchanged over such a wide stoichiometry window as [Fe_2Ge,$Fe_{1.1}Ge$]. Nevertheless Starke *et al.*[26] obtained an analogous result in the case of thin *unreconstructed* Fe-Si films that were epitaxially grown by codeposition on Si(111) with the (same) cubic CsCl structure for stoichiometry ranging from FeSi to $FeSi_2$ (just mentioned above). They found indeed that RT (1×1)-FeSi (without Fe vacancy) and (1×1)-$FeSi_2$ (with Fe vacancies) thin films exhibit similar LEED-$I(V)$ curves despite well distinct stoichiometry.

3. X-ray photoelectron diffraction

In order to investigate in more detail the stoichiometry dependence of the crystallographic structure, qualitative and quantitative data have been acquired with the help of *in situ* XPD and *ex situ* XRD experiments. The XPD technique has been widely applied in the past to determine local structures of epitaxial surfaces. If the surface is well ordered, the photoemission intensity of a core-level peak exhibits clear modulations versus emission angle. In particular, for high photoelectron kinetic energies ($E_C>500$ eV) strong intensity enhancements occur in the angular intensity distribution along internuclear axis, which connect the emitter atom to its nearest- and next-nearest-neighboring scatterer atoms. This effect, called *forward scattering*, corresponds to the zeroth-order approximation of the XPD phenomenon. However this simple forward-focusing picture usually cannot explain all the diffraction structures of the polar scan and multiple-scattering effects have to be considered. It is worth noting that XPD is more bulk sensitive than LEED, and the coherence length is of the order of the inelastic electron mean free path ($\sim$10–20 Å) whereas LEED pattern arises from electrons coherently backscattered by large ordered domains (>100 Å). We have recorded Fe $3p$ ($E_C\sim1433$ eV), Fe $2p_{3/2}$ ($E_C\sim780$ eV), Ge $3d$ ($E_C\sim1458$ eV), and Ge $3p$ ($E_C\sim1365$ eV) XPD polar plots in different high symmetry planes of the Fe-Ge film. We found first (not shown here) that, for any composition between Fe_2Ge and $Fe_{1.1}Ge$, the polar plots are nearly identical every 60° step rotation of the azimuthal orientation, which is consistent with the hexagonal symmetry of the β and η phases. Figure 5 shows the Fe $3p$ [Fig. 5(b)] and Ge $3d$ [Fig. 5(c)] core-level intensities versus polar angle along the $[1\bar{1}0]$ symmetry line of the germanium substrate measured for four distinct compositions between Fe_2Ge and $Fe_{1.1}Ge$. We focus here only on this azimuth because it coincides to the β and η phase planes of highest symmetry (see below), and the results inferred from the XPD analysis in this azimuth are fully consistent with those collected in other azimuths. Note also that we have restricted here the XPD analysis to the [Fe_2Ge,$Fe_{1.1}Ge$] composition range since XPD profiles are significantly different outside this range confirming the LEED data described before and the XRD analysis (see below). A much more detailed XPD analysis will be published elsewhere. It can be seen immediately that the polar angle distributions of the Fe $3p$ and Ge $3d$ photoelectron intensities are sharp and contrasted confirming the high crystallinity of the samples. For each Fe $3p$ and Ge $3d$ photoelectron line the four angular profiles are very similar to each other. It indicates that the local order around Fe atoms and the one around Ge atoms as well hardly change with composition in this azimuth. Let us now comment first on the Fe $3p$ core line scans. All the Fe polar scans show a series of pronounced peaks at normal emission ($\theta=0°$), at $\sim$25°, and $\sim$59°. The main differences between the Fe scans reside in the shape of the broad structure centered around 39° and the amplitude of the different peaks. The amplitude of a peak can be characterized by an anisotropy factor F defined as $F=(I_{max}-I_{min})/I_{max}$, where I_{max} is the maximum intensity of the peak and I_{min} is the minimum located immediately close to the peak. We found that the F factors are quite the same for Fe_2Ge, $Fe_{1.7}Ge$, and $Fe_{1.4}Ge$ compositions, with $F=50(\pm2)\%$ and $F=28(\pm5)\%$ for the two most marked peaks at 0° and $\sim$59°, respectively. These factors are significantly reduced for the composition $Fe_{1.1}Ge$ with $F\sim40\%$ and $F\sim10\%$ at 0° and 59°, respectively. The results are slightly different for the Ge $3d$ polar scans as we will discuss now. All the Ge polar scans show a series of marked peaks at 0°, $\sim$25°, $\sim$40°, and $\sim$59°. We clearly observe that, for each peak, the amplitude is larger for Fe_2Ge and $Fe_{1.7}Ge$ than for $Fe_{1.4}Ge$ and $Fe_{1.1}Ge$ compositions. Indeed, the anisotropy factors decrease from $\sim$37% (at 0°), $\sim$16% (at 39°), and 17% (at 58°) for Fe_2Ge and $Fe_{1.7}Ge$ to $\sim$29% (at 0°), $\sim$8% (at 39°), and 8% (at 58°) for $Fe_{1.4}Ge$ and $Fe_{1.1}Ge$ compositions.

In order to recognize forward scattering features in the polar scans and thus associate them with internuclear axis directions, we have sketched in Fig. 5(a) a cut of the ideal (without vacancy) β-Fe_2Ge compound through the $(10\bar{1}0)$ plane. In fact, in this $(10\bar{1}0)$ azimuth, the plane contains either only Fe (Fe $2a$) atoms or a 50%-50% mixture of Fe (Fe $2d$) and Ge (Ge $2c$) atoms, but the arrangement of the atomic species is the same in both cases. In particular, we clearly see that there are three atomic rows for which an intensity peak can be produced by forward scattering of high-kinetic photoelectrons for nearest or next-nearest neighbors. These expected forward-focusing directions and the corresponding crystal low index are 0° [0001], 38.7° $[11\bar{2}1]$, and 58.4° $[22\bar{4}1]$. It turns out that, with the exception of the peak centered around 25°, the polar angles of the major peaks collected for both Fe $3p$ and Ge $3d$ lines coincide fairly well with these three forward-focusing directions. In order to see whether the peak at $\sim$25° (that we also detected in both Fe $2p_{3/2}$ and Ge $3p$ core line profiles) and/or the complex shape of the broad peak centered $\sim$39° in the case of the Fe $3p$ XPD profile are either the signature of an additional ordered Fe-Ge phase or merely result from higher-order interference effects, we have performed multiple-scattering spherical wave cluster calculations for the ideal Fe_2Ge phase, i.e., without vacancies. These calculations were carried out using a series expansion algorithm based on the Rehr-Albers separable method.[27] We used a cluster of 631 atoms with a radius of 15 Å. The multiple-scattering expansion was truncated at order 4. As can be seen in Figs. 5(b) and 5(c), there is a good agreement between the calculated curve and the experimental profile (in particular for the Fe_2Ge and $Fe_{1.7}Ge$ compositions) for both Fe $3p$ and Ge $3d$ core lines. Whatever the core line, the calculated modula-

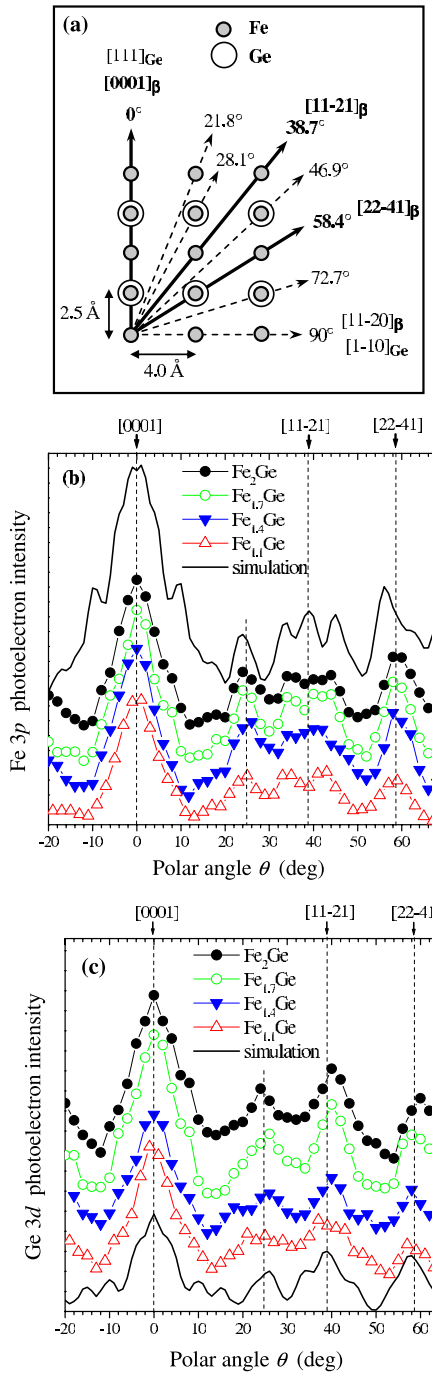

FIG. 5. (Color online) (a) Cut through the $(10\bar{1}0)$ plane of the ideal (without vacancy) β-Fe_2Ge phase. This plane contains either only Fe atoms or a 50%-50% mixture of Ge and Fe atoms. The arrows indicate crystallographic directions corresponding to forward scattering at nearest and next-nearest neighbors. (b) Calculated and experimental XPD polar scans of the Fe $3p$ core line in the azimuthal $(10\bar{1}0)$ plane from the [0001] surface normal (θ =0°) toward the $[11\bar{2}0]$ direction (θ=0°). The calculated curve (line) corresponds to the ideal β-Fe_2Ge phase. The experimental data have been collected for samples with the same nominal Fe coverage ($t_{Fe}\sim 40$ ML) but with four distinct compositions: Fe_2Ge, $Fe_{1.7}Ge$, $Fe_{1.4}Ge$, and $Fe_{1.1}Ge$. The experimental spectra are normalized to the same intensity at normal emission (θ=0°) but shifted vertically for clarity. (c) Same as in (b) but for the Ge $3d$ core line.

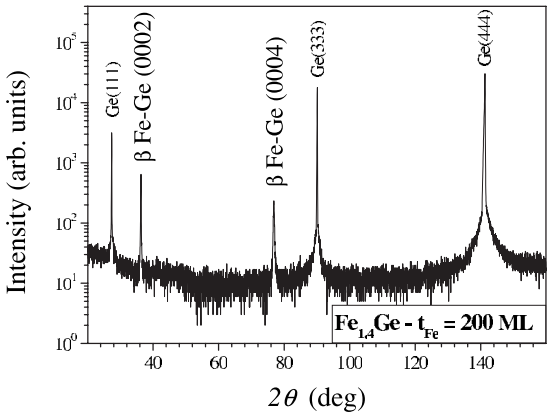

FIG. 6. θ-2θ x-ray diffraction scan for a thin film (t_{Fe} =200 ML) of $Fe_{1.4}Ge$ composition. Collected with a monochromatized Cu source.

tions are clearly sharper than the experimental ones for the whole profile since the calculations do not take into account the angular acceptance of the analyzer which is estimated between 1° and 2°. This allows us to show that the broad peak centered at ~40° (for the Fe $3p$ core line) exhibits a triple-peaked structure (for the calculated curve) that results from interference effects due to neighboring atoms located on both sides of the $[11\bar{2}1]$ atomic row. Similar splitting effects have been previously reported in the literature.[28] Note also that the angular position shift of the forward-focusing $[22\bar{4}1]$ direction (at ~56° for the calculations instead of the expected 58.4°) for the Fe core line profile is not understood yet. We think that the above mentioned slight modifications of the Fe $3p$ and Ge $3d$ core line polar profiles when the composition changes from Fe_2Ge-$Fe_{1.7}Ge$ to $Fe_{1.4}Ge$-$Fe_{1.1}Ge$ merely originate from local distortion of the hexagonal Ni_2In structure. Indeed, the systematic reduction of the overall XPD anisotropy clearly visible when we compare the Fe_2Ge and $Fe_{1.7}Ge$ Ge $3d$ profiles with respect to the $Fe_{1.4}Ge$ and $Fe_{1.1}Ge$ ones suggests an increase in static disorder. Thus, from the XPD data at hand, it is reasonable to assume that, first, the film contains only one *ordered* phase over the whole $[Fe_2Ge, Fe_{1.1}Ge]$ composition range and, second, this phase has a structural order similar to the one of the hexagonal Ni_2In phase. Lastly, the epitaxial relationships between the Fe-Ge film and the Ge substrate were determined from the comparison between the substrate and the Fe-Ge overlayer polar scans. It turns out that (0001)Fe-Ge∥(111)Ge and $[11\bar{2}0]$Fe-Ge∥$[\bar{1}10]$Ge.

4. X-ray diffraction and discussion

Figure 6 shows a typical XRD θ-2θ spectrum measured on a relatively thick (200 ML Fe coverage) $Fe_{1.4}Ge$ film with a monochromatized Cu (λ=1.540 56 Å) source. For the thinnest germanide films (typically for coverage below 40 ML) it was necessary to collect the spectrum with unmonochromatized Cu source in order to obtain sufficiently intense signal to noise ratio. Besides the three lines—(111), (222), and (333)—of the Ge substrate, the spectrum clearly exhibits two peaks centered on about 36° and 77°. As indicated these

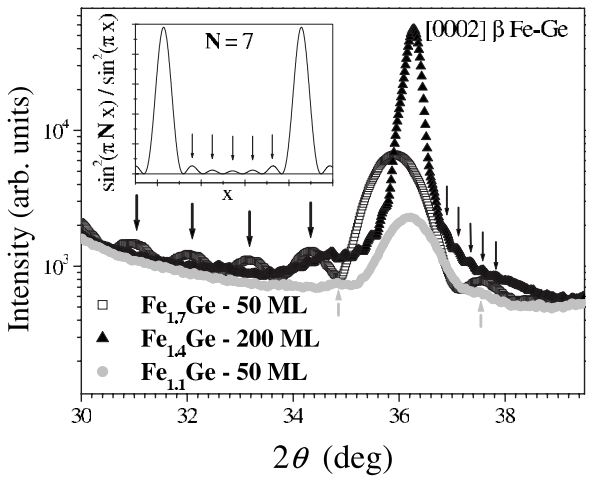

FIG. 7. θ-2θ x-ray diffraction scan around the Fe-Ge[0002] diffraction line for Fe-Ge thin layers with distinct composition and thickness. Collected with an unmonochromatized Cu source. The arrows mark the Laue oscillations. Inset: Laue function calculated for $N=7$ periodic meshes along one direction (x). The Laue oscillations between two main diffraction peaks are marked by arrows.

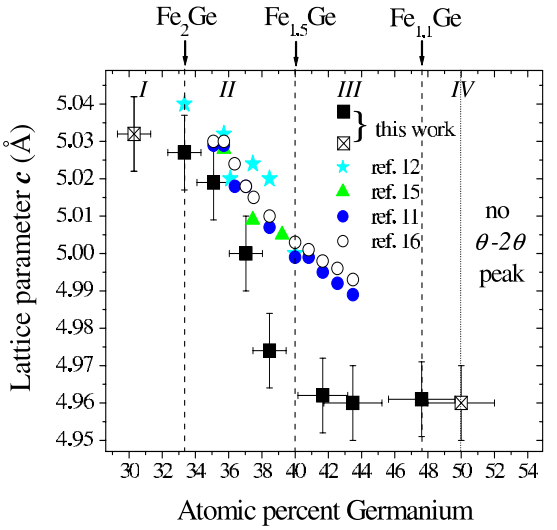

FIG. 8. (Color online) Evolution of the out-of-plane lattice parameter c versus stoichiometry for thin (t_{Fe} around 50 ML) Fe-Ge films on Ge(111). This parameter has been measured from the position of the [0002] and [0004] lines in the θ-2θ XRD scan. c values reported in the literature in the case of macroscopic ingots are also displayed for comparison. In regions II and III (full squares) only the β-derived phase is present. In region I (crossed squares) this phase is still present but the [0002] and [0004] line areas are drastically reduced with respect to the ones in regions II and III.

two peaks correspond to the (0002) and (0004) diffraction lines of the β-Ni_2In phase, respectively. Although XRD measurements in the Bragg-Brentano θ-2θ configuration probe only the periodicity along the surface normal, the absence of any additional peak (even with the highest flux) in this geometry for all samples within the $[Fe_2Ge, Fe_{1.1}Ge]$ composition range suggests that only the hexagonal Ni_2In phase is present in the layer. This result is in support to the XPD analysis. In order to get additional information on the crystalline quality of the films we have determined the vertical coherent length ($L_\perp$) that is the mean length along the surface normal for which the planes diffract coherently. The vertical coherence length has been calculated by two independent methods, first, with the help of the Scherrer formula that connects $L_\perp$ to the full width at half maximum of the Bragg peak. This method is usually employed and gives accurate $L_\perp$ value for thickness between 3 and 500 nm typically. The second method is obtained by considering the small Laue oscillations (if any) localized on both sides of the Bragg peak and required in our case to work with the unmonochromatized source for getting intense signal. More precisely if the crystal consists of N meshes with parameter d along one direction, x for instance, then the intensity of the diffracted beam is given by the Laue function $L(x) = \sin^2(\pi N x)/\sin^2(\pi x)$. Its representative curve for $N=7$ is depicted in the inset of Fig. 7. We can see that the Laue oscillations between the main peaks are separated by a fixed distance Δ. This distance is related to N and d by $N \times \Delta = d$. Let us consider now the θ-2θ XRD spectra of the 50 ML $Fe_{1.7}Ge$, 200 ML $Fe_{1.4}Ge$, and 50 ML $Fe_{1.1}Ge$ samples around the peak position Fe-Ge(0002) (Fig. 7). For each spectrum, oscillations are visible on both sides of the main peak indicating the good crystallinity along the surface normal. In fact, we found that the vertical coherence lengths measured by the two methods are nearly identical and are as large as the total thickness (estimated with the quartz microbalance) of the germanide layer. It means that the out-of-plane order is coherent over all the film thickness. We have also collected for some "thick" ($t_{Fe} \sim 200$ ML) germanide layer XRD spectra in the *rocking curve* geometry at the (0002) and (0004) peak positions (not shown here) in order to get the mosaicity and the lateral coherence length. Values around 0.3° and 20–30 nm, respectively, have been obtained, which confirm the high crystallinity for the whole $[Fe_2Ge, Fe_{1.1}Ge]$ stoichiometry range.

As clearly visible in Fig. 7, the angular position of the (0002) peak depends on the sample, suggesting a composition dependence and/or a thickness dependence of the out-of-plane lattice parameter. We have calculated this parameter that corresponds here to the lattice constant c using the two—(0002) and (0004)—Bragg peaks. Note also that with the help of the three very narrow Bragg peaks from the Ge substrate we could have calibrated the peak positions of all samples with a high accuracy. Thus the out-of-plane parameter c was determined with a high precision ($<1\%$). The lattice parameter c values as a function of stoichiometry are reported in Fig. 8. It is noteworthy that these values have been collected for the same nominal Fe coverage, of about 50 ML. Figure 8 clearly shows that the lattice constant variations can be divided into two distinct parts. In the first region (labeled II) the lattice constant decreases continuously when increasing the Ge content from 33% (Fe_2Ge) to 40% ($Fe_{1.5}Ge$). In the second region (labeled III) c is nearly constant between $Fe_{1.5}Ge$ and $Fe_{1.1}Ge$. For Ge content higher than about 50% (region IV), only the diffraction peaks from the Ge substrate were detected in the θ-2θ scan. As no LEED diffraction could also be detected for this composition region, it is likely that the Fe-Ge layers are amorphous for Ge

content above 50%. On the other side of the [Fe_2Ge, $Fe_{1.1}Ge$] range, the (0002) and (0004) aforementioned peaks are still visible up to stoichiometry around $Fe_{2.3}Ge$. These peaks are however much less intense (peak area divided by about 100) and broader than the ones in regions II and III. Thus, the $InNi_2$-type phase is still present but the major part of the film crystallizes in another structure whose determination is beyond the scope of this paper.

Let us compare now the composition dependence of the lattice parameter c of our epilayers in region II with the results previously reported in the case of macroscopic single-crystal ingots (Fig. 8). A similar but slightly less pronounced decrease of c with increasing Ge content was also found for the ingots. This decrease merely results from the reduction of the Ni_2In-derived β phase unit cell volume with increasing Ge atomic percent. Indeed as mentioned in Sec. I the β structure is stabilized through the progressive substitution of vacancies for the Fe 2d atoms when the composition evolves from Fe_2Ge to $Fe_{1.5}Ge$. In the case of A-B alloys, it has been found empirically that the substitution of B atoms for A atoms leads usually to a linear decrease (increase) of the lattice parameters if B is smaller (bigger) than A. Despite small deviations from this linear variation (the so-called Vegard law) have been reported for different systems, the continuous decrease or increase of the lattice parameters versus stoichiometry always occurs for a given stoichiometry range. In the case of the macroscopic Fe-Ge ingots, the lattice parameter a follows the same variations as c (the ratio c/a remains nearly constant to 1.25) for any composition between Fe_2Ge and $Fe_{1.5}Ge$ [compare Figs. 1(b) and 8]. Although it was not possible with our STM, LEED, and TEM techniques to measure the in-plane parameter a with a sufficient accuracy in order to probe its concentration dependence, it is reasonable to assume that the continuous formation of vacancies (with increasing Ge content) leads also to a continuous decrease of the volume of the unit cell. But in our case, the in-plane lattice parameter of the thin germanide layer is undoubtedly different from the one of the bulk compound with the same stoichiometry. Indeed for the [Fe_2Ge, $Fe_{1.1}Ge$] composition range the mismatch (m) between the germanide compound and the Ge substrate is very small, lying between about +1.3% (for $\sim Fe_{1.9}Ge$) and −0.3% (for $\sim Fe_{1.5}Ge$) as displayed in Fig. 1(b). For such a small value it is likely that the germanide layers grow coherently (i.e., homogeneously strained with its lateral lattice parameter perfectly matched to the substrate lateral lattice parameter) on the substrate up to a critical thickness (that depends of course on the stoichiometry) above the thickness of the layers investigated here. That is, our thin (total thickness smaller than 10–15 nm) layers should be coherent (undoubtedly for m values between −0.3% and +0.3%) or at least partially relaxed (plausible for m values higher that ~1%). By taken into account the in-plane lattice parameter a values of the bulk Fe-Ge compounds and the substrate in-plane lattice parameter as well, we may therefore assume that our thin Fe-Ge layers are under compressive strain up to about 38(±1)% Ge ($\sim Fe_{1.63\pm0.07}Ge$ composition) and under tensile strain for further Ge content. Thus, if our thin layers have the same density as the bulk ingots, we would expect that the decrease of c with increasing Ge content is more marked in the case of our thin layers than for the macroscopic ingots, which is actually the case. However, we also expected a higher value of c for the in-plane compressed layers than for the ingots at variance with the data of Fig. 8. Different propositions could be speculated to explain this. It is first possible that we underestimated slightly the Ge content in our thin films. Nevertheless as both the Ge and Fe evaporation rates were measured with the same (water-cooled and stable) microbalance, we think that the ratio between these two incident fluxes is estimated with a high precision. It is therefore reasonable to admit that the stoichiometry is well determined *before* the annealing treatment. On the other hand a slight increase of the Ge content through the diffusion of Ge atoms from the substrate into the germanide layer during the annealing procedure is not impossible. Our recent magnetic neutron measurements (not shown here) indicate however that the annealing does not affect the Fe magnetic moment, which suggests that the influence of the annealing on the stoichiometry is negligible. Therefore we believe that the fact that the c parameter of our in-plane *compressed* layers is slightly lower than the c values measured for the ingots indicates that the thin films are either slightly denser than the ingots (not perfect single crystal) and/or fully relaxed (very unlikely).

We will now discuss the c variations in region III. At first sight the fact that c remains constant for such a wide composition range is rather surprising. Indeed, bearing in mind the earlier discussion we could have expected that the unit cell volume and therefore the c parameter continue to shrink with further vacancy formation. However, it is noteworthy to recall that the empirical Vegard law was observed in the case of substitution of one type of atom A for another atom B and was valid only up to a limited B atom concentration. Despite a widespread of conflicting results concerning the atom or vacancy site distribution in the case of the bulk β-phase Fe-Ge (stabilized only for composition between Fe_2Ge and $Fe_{1.5}Ge$), it is very likely that the vacancies are located only on the Fe 2d sites for composition up to $Fe_{1.6}Ge$.[11,18] That is, for composition between Fe_2Ge and $Fe_{1.6}Ge$ the Fe 2d site is occupied either by a Fe atom or by a substitutional vacancy. It was found that by increasing further the Ge concentration Ge atoms start to occupy also the Fe 2d sites for compositions between $Fe_{1.6}Ge$ and $Fe_{1.5}Ge$. At higher content (between $Fe_{1.45}Ge$ and $Fe_{1.3}Ge$), the occupation rate of the Fe 2d sites by Ge atoms increases further, but Kanematsu[11] also found that the vacancies start to occupy the Fe 2a sites. It means that the substitution mechanism changes significantly around $Fe_{1.55(\pm0.1)}Ge$ in the case of the macroscopic single-crystal ingots. To these particular vacancies distributions on both sides of this $Fe_{1.55(\pm0.1)}Ge$ composition are associated specific atomic shifts. This leads to the structural transformation from the β phase to the η phase which is only an ordered superstructure of β.[11] Thus, by taking into account these data, we speculate that the drastic deviation from the Vegard law around the critical composition $Fe_{1.5}Ge$ is also the result of a modification of the vacancy formation mechanism but with no change of the hexagonal symmetry. However, different features seem to indicate that the statistical atomic or vacancy site distribution may be different in our case than for the ingots. First, in region III the lattice parameter c of the ingots is larger than the one of our epilayers.

Second, the hexagonal phase is stabilized up to the $Fe_{1.1}Ge$ composition, i.e., for significant higher Ge content as the stability range of the η phase. Again, these two facts likely could be the results of the (pseudo)coherent growth of the present thin layers. Indeed, from Fig. 1(b) it is reasonable to assume that these thin pseudomorphic films are under in-plane tensile strain ($\sim -0.3\%$ mismatch). Consequently, from linear elasticity, c is reduced to compensate this tensile strain. It is well know that in the case of relatively large misfit (typically above a few percent) between the expected bulk phase and the substrate the epitaxial overlayer may adopt a crystal structure that differs from the bulk phase but which is well lattice matched to the substrate. If we look at the bulk phase diagram in Fig. 1(b) it appears that for Ge content around 45% the stable phase is Fe_6Ge_5. Its space group symmetry is monoclinic ($C2/m$) and the cell parameters are $a=9.965$ Å, $b=7.826$ Å, $c=7.801$ Å, and $\beta=109.67°$.[16] As mentioned in Sec. I, this cell corresponds to a strongly distorted β phase with $c=4.983$ Å, $b=3.913$ Å (-2.4%), and $a=4.162$ Å ($+3.84\%$). The epitaxial growth of this phase is therefore unexpected on Ge(111). Thus, it is possible that our thin germanide layers are stabilized and keep the same hexagonal symmetry in the whole region III, thanks to the coherent growth. It is rather amazing that c and a (thus, the cell volume) do not vary with stoichiometry in region III. A possible explanation is that within this stoichiometry range the Ge concentration increase in the cell is due to vacancy formation (mainly on the Fe $2d$ sites) up to a critical composition and results from the Ge atom substitution for Fe for higher Ge content.

To summarize, XPD, TEM, and θ-2θ XRD analyses show that the thin layers adopt a defect $InNi_2$-$B8_2$ structure of hexagonal symmetry similar to the bulk β-Fe-Ge phase but over a wider stoichiometry range—extending from Fe_2Ge to $Fe_{1.1}Ge$—than in the case of single-crystal macroscopic ingots. This remarkable result may be the consequence of the thin layer pseudomorphic growth on the Ge(111) substrate. Such a wide composition range of stability implies that the local order within the cell must change with stoichiometry. It has been qualitatively confirmed by both the XPD and XRD data. In particular the XPD modulations are significantly attenuated for compositions between $Fe_{1.4}Ge$ and $Fe_{1.1}Ge$ in comparison to the modulations for lower Ge content. This suggests that the local atomic order both around the Fe atoms and around the Ge atoms is the lowest for this composition. It likely results from marked atomic site shifts with respect to the ideal β-Fe_2Ge phase due to the vacancy formation. Indeed, Albertini *et al.*[18] found that for macroscopic ingots of $Fe_{1.67}Ge$ composition the Ge atom is slightly displaced (about 0.2 Å) from the ($2c$) site toward an adjacent vacancy in a ($2d$) site. For higher Ge concentration we may speculate that slight atomic displacements also occur along the [0001] direction. This is qualitatively supported by the XRD spectra in Fig. 7. Indeed, the Laue oscillations are much more damped (and the background of the main peak is enhanced) for the $Fe_{1.1}Ge$ composition than for the $Fe_{1.7}Ge$ stoichiometry, indicating that the atomic disorder in the out-of-plane direction is more pronounced for $Fe_{1.1}Ge$ than for $Fe_{1.7}Ge$.

Another striking finding is that, though the hexagonal symmetry does not change with stoichiometry within the wide [Fe_2Ge,$Fe_{1.1}Ge$] window, the surface periodicity suddenly changes around the critical composition $Fe_{1.5}Ge$. Moreover, the stoichiometry dependence of the c out-of-plane parameter is also strongly modified at the *same* critical stoichiometry. As this stoichiometry is identical to the one for which the macroscopic ingot structure evolves from the hexagonal β phase toward the hexagonal η phase, it is tempting to assert that the surface periodicity change is a fingerprint of this β-η phase transformation. Since the $(\sqrt{3}\times\sqrt{3})R30°$ periodicity remains up to significantly higher Ge concentration than the maximum Ge concentration for which the η phase still exists in the bulk phase diagram we prefer however to remain cautious. We just speculate that the periodicity change around 40% Ge atomic percent ($\sim Fe_{1.5}Ge$ composition) could arise from a minor modification of the local atomic order (through tiny displacements of both Fe and Ge atomic positions) due to a subtle modification of the Fe site occupation (via Fe vacancy formation or Ge substitution for Fe) mechanism at this critical stoichiometry as mentioned earlier.

B. Magnetic properties

1. Curie temperature

We have studied the onset of ferromagnetic order and the magnetic anisotropy in the thin Fe-Ge films as a function of stoichiometry and thickness. Kerr magnetization loops (not shown) collected both in polar and longitudinal geometries clearly indicate that the magnetic easy axis lies in the film plane for all the ferromagnetic samples investigated here. It means that the out-of-plane c axis is the hard axis of magnetization, in agreement with torque measurements previously performed on macroscopic single-crystal β-Fe-Ge ingots.[8,29,30] Thus, we could have determined the Curie temperature (T_C) from the thermal variations of the longitudinal Kerr amplitude measured in an external magnetic field of ± 100 Oe amplitude, which is well larger than the tiny in-plane saturation field (≤ 10 Oe). Indeed the Kerr amplitude decreases continuously with increasing temperature [see Fig. 3b in Ref. 7] and vanishes at a critical temperature that we define as the Curie temperature, as usually done in the literature. We found that for a fixed stoichiometry T_C increases continuously with the layer thickness. It is shown in the inset of Fig. 9 for the $Fe_{1.7}Ge$ ($\sim Fe_{63}Ge_{37}$) composition. Note that the onset of long-range ferromagnetic order occurs around ~ 5 ML Fe coverage, i.e., in the vicinity of the percolation threshold of the flat Fe-Ge islands. Such a monotonous T_C increase with increasing thickness has been observed previously in a lot of ferromagnetic thin films.[31] It results from finite size effect.[32] In order to determine the Curie temperature versus stoichiometry we have therefore chosen a sufficiently large film thickness (~ 30 ML Fe coverage) for which T_C should be close to the one of infinite thickness layer. Figure 9 shows the variation of T_C as a function of stoichiometry. We observe immediately that long-range ferromagnetic order may be present over the wide [Fe_2Ge,$Fe_{1.1}Ge$] composition range for which the Fe-Ge layer is homogeneous and crystallizes in the (pseudo-)Ni_2In-derived structure. We also see that T_C con-

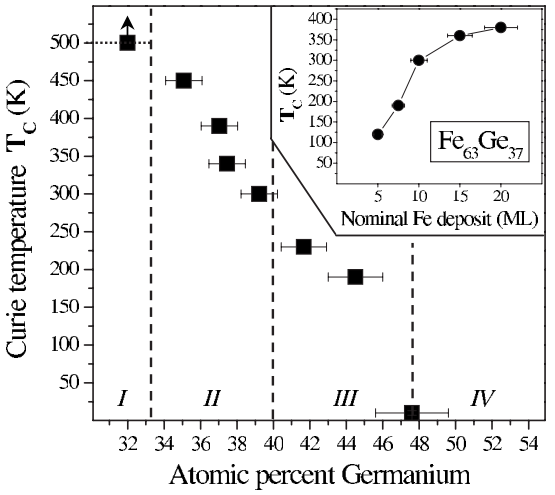

FIG. 9. Variations of the Curie temperature (T_C) for thin (t_{Fe} ~30 ML) Fe-Ge epilayers as a function of Ge content. The four regions labeled I–IV correspond to the ones in Figs. 3 and 8. For Ge content below about 33% T_C is above 500 K, the maximum temperature that we can reach with our Kerr setup. Inset: evolution of T_C as a function of nominal Fe coverage for the composition $Fe_{63}Ge_{37}$ (~$Fe_{1.7}Ge$).

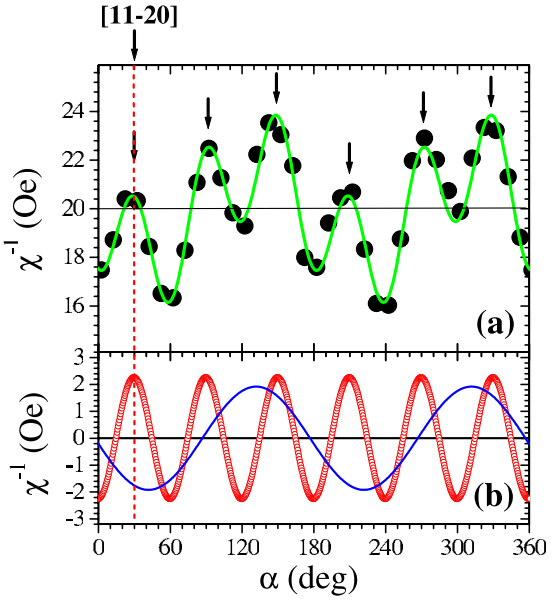

FIG. 10. (Color online) (a) Experimental inverse susceptibility χ^{-1} (filled black circles ●) versus in-plane angle α for a thin (t_{Fe} =50 ML) $Fe_{1.8}Ge$ film. The transverse static bias field H_{per} amplitude is 20 Oe. α=30° corresponds to the [11$\bar{2}$0] direction. One notes four major maxima at $\alpha \approx 90°$, 150°, 270°, and 330° and two minor maxima at $\alpha \approx 30°$ and 210°. The Fourier analysis gives the following twofold and sixfold anisotropy fields: K_U/M_S=0.9 Oe and K_6/M_S=6.7 Oe and the easy axis associated to the sixfold symmetry magnetic anisotropy is along the equivalent ⟨11$\bar{2}$0⟩ directions. The curve (full green line) is a simulation using the determined anisotropy constants K_U and K_6 and taking into account the amplitude and phase of the Fourier spectrum for both second- and six-order components. (b) Simulations corresponding either only to the second-order component (full blue line) or only to the sixth-order component (open red circles ○).

tinuously decreases with increasing Ge content. It results merely from the progressive reduction of the Fe neighbor coordination number of the Fe atoms with decreasing Fe content. The most interesting result is that the Curie temperature for the Fe-rich $Fe_{1.9}Ge$ composition is above 450 K, i.e., well above RT. For still Fe-richer thin film (region I), the Curie temperature could not be determined since it is higher than 500 K which is the maximum temperature we can reach with our setup. Figure 9 also shows that no long-range ferromagnetic order exists for Ge content above ~48%.

2. In-plane magnetic anisotropy

As we mentioned above all the samples investigated here have an in-plane magnetic easy axis. Longitudinal Kerr loops showed that the saturation field amplitude is less than 10 Oe for any sample orientation with respect to the field direction. Consequently, the in-plane magnetic anisotropy is very small. To determine it precisely we have performed TBIIST measurements. Let us first summarize the principle of the TBIIST method described in more detail in Ref. 22. The TBIIST—for transversely biased initial inverse susceptibility (χ^{-1}) and torque (ΔH)—measurements have been carried out with a standard MOKE setup in a longitudinal configuration but under an in-plane static bias field H_{per} applied perpendicular to the longitudinal sweep field H. The data around M_L=0 (M_L is the longitudinal component of the magnetization) are collected and the two quantities χ^{-1} (inverse susceptibility) and ΔH (sweep field offset at M_L=0) are determined. It can be shown that a Fourier analysis of the variations of $\chi^{-1}(\alpha)$ and $\Delta H(\alpha)$ versus the angle α between H_{perp} and a reference direction in the film plane gives in two independent ways the symmetry, magnitude, and direction of the in-plane magnetic anisotropy contributions.[22] As an example the variation of χ^{-1} versus α for a sample of $Fe_{1.8}Ge$ (with about 50 ML Fe coverage) is reported in Fig. 10. It appears clearly that $\chi^{-1}(\alpha)$ is an oscillating function around a mean value corresponding to the intensity of the in-plane static bias field H_{per} (20 Oe in the present case). More precisely, the curve exhibits clearly a sixfold symmetry but with nonequivalent amplitude for the six maxima indicating the presence of other anisotropy contributions. In fact, by performing the Fourier analysis of $\chi^{-1}(\alpha)$ we found that a tiny contribution of twofold symmetry is also present. This is illustrated in Fig. 10 by the fact that the addition of the two Fourier components, of second and six orders, fits nicely the experimental curve. It shows clearly that the in-plane magnetic anisotropy is the superposition of the hexagonal sixfold and uniaxial contributions. From the amplitudes of the Fourier spectra determined from $\chi^{-1}(\alpha)$ data we found that the field amplitude of the sixfold symmetry anisotropy is about 7 Oe and its corresponding easy axis lies *always* along the ⟨11$\bar{2}$0⟩ directions, confirming the magnetocrystalline origin of this anisotropy component. Note that torque measurements performed on β Fe-Ge macroscopic ingots showed also that the *a* axis is the easiest direction in the basal plane.[8,29] As to the uniaxial component, its field amplitude is also very small (less than 2 Oe) but, unlike the sixth-order

contribution, is not related to any crystallographic sample direction. The origin of this tiny uniaxial anisotropy is not yet clear but may be due to the small vicinality ($\sim 0.3°$) of the nominal Ge(111) wafer surface.

IV. SUMMARY AND CONCLUSION

The growth, structure, and magnetism of thin (total thickness below 40 nm) Fe-Ge films synthesized by MBE codeposition on Ge(111) have been investigated as a function of stoichiometry and thickness. Detailed STM, LEED, XPD, and θ-2θ XRD measurements showed that for a wide composition range extending from about Fe_2Ge to $Fe_{1.1}Ge$ the layer is homogeneous, atomically flat, and well crystallized. It adopts a crystallographic structure of hexagonal symmetry, which is derived from the $B8_2$ (Ni_2In) structure. The epitaxial orientation between the Ge substrate and the Fe-Ge layers is $(0001)_{Fe\text{-}Ge} \| (111)_{Ge}$ and $[11\bar{2}0]_{Fe\text{-}Ge} \| [\bar{1}10]_{Ge}$. It was found however that (i) the surface periodicity reflected by LEED and STM and (ii) the amplitude of the out-of-plane lattice parameter c vary within this composition range. Indeed two distinct stoichiometry regimes appear on both sides of the critical stoichiometry $Fe_{1.5}Ge$ (about 40% atomic Ge). From Fe_2Ge to $Fe_{1.5}Ge$ (region II) the surface periodicity is $p(2 \times 2)$ and c continuously decreases with Fe content, whereas from $Fe_{1.5}Ge$ to $Fe_{1.1}Ge$ (region III) the surface periodicity is $(\sqrt{3} \times \sqrt{3})R30°$ and c remains constant. These features have been interpreted as a clear fingerprint of a tiny transformation of the crystalline structure but without any change in symmetry. In particular θ-2θ XRD and XPD experiments showed an increase of the local atomic disorder from region II to region III. As this critical composition coincides to the ones for which it has been previously reported that macroscopic Fe-Ge ingots undergo a transition between the β and η hexagonal parent phases, it is possible that the same occurs for our thin Fe-Ge epilayers. Detailed XRD measurements on thicker films should be performed to eventually explore this tiny structural transformation. On both sides of the wide $[Fe_2Ge, Fe_{1.1}Ge]$ composition range the layer is no more homogeneous. More precisely, for higher Fe content the film contains both the above mentioned Ni_2In-derived phase and a Fe-richer phase (probably bcc Fe), whereas for higher Ge content the layer is amorphous.

Magnetic characterization showed that the thin Fe-Ge layers are ferromagnetic up to about 48 at. % Ge. Interestingly, the Curie temperature of the homogeneous Ni_2In-derived epilayers is tunable between about 7 K ($\sim Fe_{1.1}Ge$ composition) and 450 K ($\sim Fe_{1.9}Ge$ composition) with increasing Fe content. Finally the magnetic easy axis of this homogeneous phase lies in the film plane as found previously in the case of β Fe-Ge macroscopic ingots. More precisely, a small uniaxial anisotropy is superimposed on a sixfold order one that results from the hexagonal symmetry of the crystallographic structure. Finally, since the synthesis of this single-crystal Ni_2In-derived phase is very quicker and easier as thin epilayers than as macroscopic ingots it opens the way to reinvestigate the controversial results reported previously on some magnetic properties of this phase.

ACKNOWLEDGMENTS

The authors are very grateful to J. Baron and G. Schmerber for XRD data. We also wish to thank Y. Nehme, A. Medahoui, S. Hajjar, L. Chaput, C. Pirri, J.-L. Bubendorff, and C. Uhlaq-Bouillet for contributions to this work. It is a pleasure to thank E. Denys for his expert technical assistance. Financial support from Centre National de la Recherche Scientifique (CNRS) and Région Alsace is gratefully acknowledged.

*Corresponding author; guillaume.garreau@uha.fr

[1] D. M. Gillingham, M. Tselepi, A. Ionescu, S. J. Steinmuller, H. E. Beere, D. A. Ritchie, and J. A. C. Bland, Phys. Rev. B **76**, 214412 (2007); B. Roldan Cuenya, A. Naitabdi, E. Schuster, R. Peters, M. Doi, and W. Keune, *ibid.* **76**, 094403 (2007), and references therein.

[2] M. Marangolo, F. Gustavsson, G. M. Guichar, M. Eddrief, J. Varalda, V. H. Etgens, M. Rivoire, F. Gendron, H. Magnan, D. H. Mosca, and J.-M. George, Phys. Rev. B **70**, 134404 (2004).

[3] V. F. Motsnyi, J. De Boeck, J. Das, W. Van Roy, G. Borghs, E. Goovaerts, and V. I. Safarov, Appl. Phys. Lett. **81**, 265 (2002).

[4] T. Sadoh, M. Kumano, R. Kizuka, K. Ueda, A. Kenjo, and M. Miyao, Appl. Phys. Lett. **89**, 182511 (2006).

[5] K. Hamaya, H. Itoh, O. Nakatsuka, K. Ueda, K. Yamamoto, M. Itakura, T. Taniyama, T. Ono, and M. Miyao, Phys. Rev. Lett. **102**, 137204 (2009).

[6] Changgan Zeng, S. C. Erwin, L. C. Feldman, A. P. Li, R. Jin, Y. Song, J. R. Thompson, and H. H. Weitering, Appl. Phys. Lett. **83**, 5002 (2003); C. Zeng, W. Zhu, S. C. Erwin, Z. Zhang, and H. H. Weitering, Phys. Rev. B **70**, 205340 (2004).

[7] R. Jaafar, Y. Nehme, D. Berling, J. L. Bubendorff, A. Mehdaoui, C. Pirri, G. Garreau, and C. Uhlaq-Bouillet, Appl. Phys. Lett. **93**, 033114 (2008).

[8] H. Katsuraki, J. Phys. Soc. Jpn. **19**, 863 (1964).

[9] J. B. Forsyth and P. J. Brown, *Proceedings of the International Conference of Magnetism* (Institute of Physics, London, 1964), p. 524.

[10] K. Yasukochi, K. Kanematsu, and T. Ohoyama, J. Phys. Soc. Jpn. **16**, 429 (1961).

[11] K. Kanematsu, J. Phys. Soc. Jpn. **20**, 36 (1965).

[12] E. Adelson and A. E. Austin, J. Phys. Chem. Solids **26**, 1795 (1965).

[13] M. Richardson, Acta Chem. Scand. (1947–1973) **21**, 2305 (1967).

[14] G. A. Fatseas, J.-L. Dormann, and L. Brossard, J. Phys. Colloq. **32**, 785 (1971).

[15] P. J. Schurer, N. J. G. Hall, and A. H. Morrish, Phys. Rev. B **18**, 4860 (1978).

[16] B. Malaman, J. Steinmetz, and B. Roques, J. Less-Common Met. **75**, 155 (1980).

[17] F. Albertini, A. Deriu, D. Negri, A. Paoluzi, L. Pareti, M. Monciardini, G. Calestani, O. Moze, and R. Sonntag, J. Magn. Magn. Mater. **157-158**, 655 (1996).
[18] F. Albertini, L. Pareti, A. Deriu, D. Negri, G. Calestani, O. Moze, S. J. Kennedy, and R. Sonntag, J. Appl. Phys. **84**, 401 (1998).
[19] A.-K. Larsson, S. Furuseth, and R. Withers, J. Solid State Chem. **141**, 199 (1998).
[20] x and y are therefore related by $x=(100)/(1+y)$ or $y=(100-x)/x$.
[21] MSSPEC package: Available upon request (didier.sebilleau@univ-rennes1.fr).
[22] D. Berling, S. Zabrocki, R. Stephan, G. Garreau, J. L. Bubendorff, A. Mehdaoui, P. Wetzel, D. Bolmont, C. Pirri, and G. Gewinner, J. Magn. Magn. Mater. **297**, 118 (2006).
[23] P. A. Bennett, M. Copel, D. Cahill, J. Falta, and R. M. Tromp, Phys. Rev. Lett. **69**, 1224 (1992).
[24] *Scanning Tunneling Microscopy I*, Series in Surface Science, edited by R. Wiesendanger and H.-J. Güntherodt (Springer-Verlag, Berlin, 1994).
[25] In fact each curve is an average of the four curves collected for the first-order integer—(10), (11), (01), and $(\bar{1}0)$—spots in order to take into account the tiny misalignment of the incident beam with the surface normal in our setup.
[26] U. Starke, W. Weiss, M. Kutschera, R. Bandorf, and K. Heinz, J. Appl. Phys. **91**, 6154 (2002).
[27] J. J. Rehr and R. C. Albers, Phys. Rev. B **41**, 8139 (1990).
[28] D. Agliz, A. Quémerais, and D. Sébilleau, Surf. Sci. **343**, 80 (1995).
[29] Y. Tawara, J. Phys. Soc. Jpn. **19**, 776 (1964).
[30] J. J. Becker and E. M. Symes, J. Appl. Phys. **36**, 1000 (1965).
[31] C. Liu, E. R. Moog, and S. D. Bader, Phys. Rev. Lett. **60**, 2422 (1988).
[32] G. A. T. Allan, Phys. Rev. B **1**, 352 (1970).